Synthetic Metals 226 (2017) 157–163

Contents lists available at ScienceDirect

Synthetic Metals

journal homepage: www.elsevier.com/locate/synmet

# Well-designed poly(3-hexylthiophene) as hole transporting material: A new opportunity for solid-state dye-sensitized solar cells

Michèle Chevrier[a,b,**], Hesham Hawashin[c], Sébastien Richeter[a], Ahmad Mehdi[a], Mathieu Surin[d], Roberto Lazzaroni[d], Philippe Dubois[b], Bernard Ratier[c], Johann Bouclé[c,*], Sébastien Clément[a,*]

[a] Institut Charles Gerhardt, Université de Montpellier, Place Eugène Bataillon, 34095 Montpellier Cedex 05, France
[b] Service des Matériaux Polymères et Composites (SMPC), Centre d'Innovation et de Recherche en Matériaux et Polymères (CIRMAP), Université de Mons – UMONS, 20 Place du Parc, 7000 Mons, Belgium
[c] Univ. Limoges, CNRS, XLIM, UMR 7252, F-87000 Limoges, France
[d] Laboratory for Chemistry of Novel Materials, CIRMAP, University of Mons UMONS, 20 Place du Parc, 7000 Mons, Belgium

ARTICLE INFO

*Article history:*
Received 13 January 2017
Received in revised form 15 February 2017
Accepted 16 February 2017
Available online xxx

*Keywords:*
Poly(3-hexyl)thiophene
Spiro-OMeTAD
Hole transporting material
ss-DSSC
AFM

ABSTRACT

All solid-state dye-sensitized solar cells (ss-DSSCs) based on the reference **D102** organic dye and using poly(3-hexylthiophene) (**P3HT**) as hole transporting material were fabricated and compared to the most used 2,2′,7,7′-tetrakis-(N,N-di-*p*-methoxyphenylamine)-9,9′-spirobifluorene (**spiro-OMeTAD**). Power conversion efficiency of 4.78% was reached with **P3HT** *vs.* 3.99% with **spiro-OMeTAD**, which emphasizes that polythiophene derivatives remain serious alternatives to **spiro-OMeTAD** for efficient and low-cost photovoltaic energy conversion. Here, **P3HT** combining high regioregularity, medium-range molecular weight and narrow dispersity was targeted. The ability of those **P3HT** chains to form semicrystalline domains upon annealing leads to improved hole mobility, photocurrent collection and thus, device performance.



## 1. Introduction

The challenges stemming from dwindling fossil resources, global population increase and environmental issues require more than ever finding cheap, sustainable and efficient alternative sources of energy. Photovoltaic cells are considered as one of the greenest ways to produce electrical energy. In this context, considerable attention is being paid on photovoltaic materials and manufacturing processes with the aim of increasing power conversion efficiency (PCE) and reducing costs. Even if silicon based solar cells have reached PCEs of 25% [1], they require expensive production processes [2]. In order to simplify the device fabrication, increase the production rate and reduce the cost, new concepts based on solution-processed photovoltaics were developed. Among these technologies, dye-sensitized solar cells (DSSCs), pioneered by Grätzel and colleagues, have attracted considerable interest due to their low-cost production over silicon photovoltaic devices [3,4].

A DSSC consists of a mesoporous nanocrystalline *n*-type semiconductor (typically $TiO_2$) sensitized with a dye, deposited onto an anode and infiltrated by a redox active electrolyte (generally triiodide/iodide ions), completed by a counter-electrode (cathode). Even if PCEs over 13% have been reached for liquid-electrolyte DSSCs [5], this technology hardly meets commercial applications due to several drawbacks, especially regarding the presence of a liquid electrolyte. Besides potential leakage issues, the commonly used $I_3^-/I^-$ system is corrosive and dissolves many of sealants and metal interconnects in the cell. Although several alternative redox couples less corrosive than iodide such as the $Co^{3+}/Co^{2+}$ [6,7] or the $Cu^{2+}/Cu^{+}$ systems have been reported [8], their long-term stability remains unproved [9]. If the devices containing these liquid electrolytes are not perfectly sealed, the liquid evaporates away and facilitates the entry of impurities such as water and oxygen [4,9]. As such, these DSSCs are not appropriate to a widespread commercialization by industry as the liquid electrolyte requires a careful packaging [9].

* Corresponding authors.
** Corresponding author at: Institut Charles Gerhardt, Université de Montpellier, Place Eugène Bataillon, 34095 Montpellier Cedex 05, France.
*E-mail addresses:* michele.chevrier@umons.ac.be (M. Chevrier), johann.boucle@unilim.fr (J. Bouclé), sebastien.clement1@umontpellier.fr (S. Clément).

http://dx.doi.org/10.1016/j.synthmet.2017.02.015
0379-6779/

Several approaches have been proposed to replace liquid electrolytes using either quasi-solid electrolyte [10–12] or solid-state hole-transporting materials (HTM) in solid-state DSSCs (ss-DSSCs) [13]. Among solid-state HTMs, 2,2′,7,7′-tetrakis(N,N-di-*p*-methoxyphenylamine)-9-9′-spirobifluorene (**spiro-OMeTAD**) remains the most successful one, owing to a number of advantages such as its glass transition temperature, its good solubility, its ionization potential, its absorption spectrum and its solid-state morphology [14]. Although **spiro-OMeTAD** HTM allows achieving PCEs up to 7.2% in classical ss-DSSCs [15], it has some drawbacks such as a quite modest hole mobility in its pristine form ($\approx 10^{-4}$ cm$^2$ V$^{-1}$ s$^{-1}$)[16] and a relatively complex multistep and expensive synthesis [17].

Consequently, conjugated polymers such as polyaniline [18,19], polypyrrole [20,21], poly(3,4-ethylenedioxythiophene) [22–24], and poly(3-hexylthiophene) (**P3HT**) [25,26] have been intensively investigated as alternative HTMs with the aim of overcoming these problems. **P3HT** exhibits a higher hole mobility as well as superior film-formation properties compared to **spiro-OMeTAD** [27,28]. Besides, the ability of **P3HT** to absorb visible light (450–600 nm) can in principle improve the light-harvesting capacity of the devices and thus, contribute to the photocurrent through charge and/or energy transfer pathways [29].

Unfortunately, the device performances obtained with **P3HT** as HTM still require improvements compared to **spiro-OMeTAD**, especially due to a reduced pore filling capacity in the mesoporous $TiO_2$ layer [30]. The size of polymer chains may limit pore filling by **P3HT** and thus, the effective thickness of the mesoporous $TiO_2$ layer [31]. This parameter is important since increasing the $TiO_2$ layer thickness would enable increasing light absorption and efficiency [31].

In this communication, we demonstrate that a specifically-designed **P3HT**, combining (i) high regioregularity, (ii) medium-range molecular weight and (iii) narrow dispersity, can be a more suitable HTM for efficient ss-DSSCs than **spiro-OMeTAD**, using a classical glass/FTO/$TiO_2$/**D102**/HTM/Au device structure. The commercially available metal free dye D102 was chosen since it exhibits high extinction coefficients (55 800 L mol$^{-1}$ cm$^{-1}$) and necessitates no additional co-adsorbent during the dye impregnation [32–34]. To provide further insight into the device operation, UV–vis absorption spectroscopy, incident photon-to-current efficiency (IPCE), atomic force and scanning electron microscopies (AFM and SEM, respectively) have been employed. To the best of our knowledge, this is the first report where **P3HT** appears as the best HTM in organic ss-DSSCs, giving a new impetus to the use of polythiophene derivatives for efficient and potentially low-cost third-generation photovoltaic cells.

## 2. Experimental

### 2.1. Materials

Titanium(IV) isopropoxide (97%, Aldrich), titanium(IV) chloride (98%, Aldrich), D102 dye (95%, Aldrich), $TiO_2$ paste (Dyesol 18NR-T, Aldrich) bis(trifluoromethane)sulfonimide lithium salt (LiTFSI) (99%, Aldrich), 4-*tert*-butylpyridine (96%, Aldrich), **spiro-OMeTAD** (99%, Solaronix), absolute ethanol were used as received without further purification. **P3HT** ($M_n$ = 23 000 g mol$^{-1}$, $M_w$ = 28 500 g mol$^{-1}$, Đ = 1.24) was prepared according to methods reported in literature [35,36]. Number-averaged ($M_n$) and weight-averaged ($M_w$) molecular weights, and molecular weight distribution (Đ) of **P3HT** were estimated using size exclusion chromatography (SEC) on a Polymer Laboratories liquid chromatograph equipped with a PL-DG802 degasser, an isocratic HPLC pump LC 1120 (flow rate of 1 mL min$^{-1}$), a Marathon autosampler (loop volume of 200 mL, solution conc. of 1 mg mL$^{-1}$), a PL-DRI refractive index detector and three columns: a PL gel 10 mm guard column and two PL gel Mixed-B 10 mm columns (linear columns for separation of molecular weight polystyrene standards ranging from 500 to $10^6$ Daltons). The eluent used was THF at a flow rate of 1 mL min$^{-1}$ at 40 °C. Polystyrene standards were used to calibrate the SEC. UV–vis spectra were recorded at room temperature on a Safas D.E.S UV–vis spectrometer.

### 2.2. Fabrication of the solar cells

Solar cells were prepared according to the following procedure [34]: FTO-coated conducting glass substrates (Solaronix) were cleaned in ultrasonic baths in water, acetone and isopropanol for 10 min each before being treated for 5 min by UV-ozone. A compact layer of $TiO_2$ was deposited by spray-pyrolysis at 450 °C from a solution of titanium isopropoxide and acetylacetone in ethanol followed by annealing at 450 °C for 20 min in air. A nanoporous $TiO_2$ layer was applied by spin-coating a solution of a commercial $TiO_2$ nanoparticle paste diluted in ethanol at a 1:1 weight ratio. The layers were then gradually annealed from 250 °C up to 500 °C over 45 min. The substrates were then treated in a 0.02 M $TiCl_4$ aqueous solution for 2 h, rinsed with water and annealed at 450 °C for 45 min. The electrodes were finally immersed in a D102 dye solution (0.3 mM) in a acetonitrile:*tert*-butanol mixture (1:1) for 15 h in the dark. After rinsing the electrodes and drying in air, HTMs were deposited by spin-coating a **spiro-OMeTAD** (200 mg mL$^{-1}$) or **P3HT** solution (25 mg mL$^{-1}$) in chlorobenzene containing tert-butylpyridine and LiTFSI as additives (LiTFSI was predissolved in acetonitrile at a concentration of 189 mg mL$^{-1}$). Gold top electrodes were finally evaporated in vacuum ($10^{-6}$ mbar) using shadow masks that define two active areas per substrate (around 0.15 cm$^2$ each).

### 2.3. Characterization of the solar cells

The current density-voltage (J-V) measurements, in the dark and under illumination, were performed in air using a Keithley model 2400 digital source meter by applying independent external voltage to the cell and by measuring the photogenerated current. The spectral mismatch between the emission of the solar simulator (NEWPORT class A, 1 600 W) and the global AM1.5G solar spectrum (IEC 60904-3 Ed.2) was corrected using a mismatch factor and the solar simulator irradiance was adjusted accordingly using a certified silicon reference cell in order to achieve an equivalent AM1.5G irradiance of one sun (100 mW cm$^{-2}$) on the test cells. The incident photon-to-current efficiency (IPCE) was estimated using a monochromated 75 W xenon lamp (Newport) in static regime, with a calibrated picoamperater (Keithley 485) and a calibrated photodiode. All data shown in this work were the average values of four independent parallel tests.

### 2.4. Fabrication of the organic field-effect transistors

Bottom gate/bottom contact prefabricated OFET substrates (Ossila) were cleaned by an ultrasonic treatment with chlorobenzene, acetone, ethanol and isopropanol for 10 min each, before being dried under nitrogen flow. The structures are based on a p-type silicon substrate as gate electrode and silicon oxide as gate dielectric. Gold drain and source electrodes, deposited on top of $SiO_2$, define a 1 mm wide and 30 μm long OFET channel. The hole transporting materials (HTMs), *i.e.* **P3HT** or **spiro-OMeTAD**, were deposited by drop-casting from a chlorobenzene solution at a concentration of 1 mg mL$^{-1}$ and the substrate was then dried in air in the dark. Additional annealing up to 150 °C for 5 min was carried out for some samples before the electrical measurements. All film deposition, annealing and current-voltage characterization were

performed in air. The surface capacitance of the gate dielectric is estimated to 10.9 nF cm$^{-2}$.

### 2.5. Characterization of the organic field-effect transistors

The output and transfer electrical characteristics of the transistors were recorded in air using a Keithley 4200 analyzer. Hole mobilities were obtained in the saturation regime of the drain-source current (IDS) by using the classical expression: $IDS = (W/2L)C_{ox}\mu_{sat}(V_{GS}-V_{th})^2$, where W/L is the channel width/length, $C_{ox}$ is the gate dielectric layer capacitance per unit area, $V_{GS}$ and $V_{th}$ are the gate and threshold voltages, respectively.

### 2.6. Atomic force microscopy

Atomic force microscopy (AFM) measurements were performed with a Nanoscope III microscope (from Bruker Nano), in tapping-mode at room temperature under ambient conditions. NCHV tips were used with nominal resonance frequency of 320 kHz. All raw AFM images were analyzed using the Nanoscope Analysis software.

### 2.7. Scanning electron microscopy

Cross-sections of the solar cell devices were imaged by scanning electron microscopy (SEM). Samples were scribed on the substrate (glass) side and cracked prior to acquisition of the SEM-images (HR-field emission gun S-4800 Hitachi microscope). Entire cross sections were imaged at a magnification of 25 000× and 20 000× for **spiro-OMeTAD** and **P3HT**-based devices, respectively. Prior to the analysis, the samples were metallized with a thin platinum layer. The acceleration voltage (EHT) was 2 kV and the working distance (WD) ranged from 5 to 8 mm.

## 3. Results and discussion

Photovoltaic cells using **D102**-sensitized $TiO_2$ as electrodes and **P3HT** or **spiro-OMeTAD** as solid HTM were fabricated following a conventional methodology and their photovoltaic properties were investigated [34]. The optical, electronic, electrochemical properties, and solid-state packing of **P3HTs** are strongly influenced by the molecular weight and dispersity [37–40]. The Kumada Catalyst Transfer Polycondensation (KCTP) method was chosen for the synthesis of **P3HT** (see Figs. S1 and S2, ESI for characterization data), because it enables chain-growth polymerization, and leads to polymer with relatively high molecular weight and narrow dispersity [41]. Wang et al. have recently reported that the best compromise between hole mobility, pore-filling and photovoltaic performances is achieved with **P3HT** HTM having medium-range molecular weight [42]. For this reason, we decided to target a **P3HT** having a medium molecular weight ($M_n$ = 23 000 g mol$^{-1}$). The dye impregnation (**D102**) was carried out in an acetonitrile/*tert*-butanol mixture at 0.3 mM for 15 h without any coadsorbent. HTM solutions were prepared in chlorobenzene with common additives (4-*tert*-butylpyridine (TBP) and bis(trifluoromethane)sulfonimide lithium salt (LiTFSI)) and stirred for 4 days at room temperature. The additives are important in ss-DSSCs for both **spiro-OMeTAD** and **P3HT** [43]. In particular, Ramakrishna et al. reported that the treatment of **D102**/**P3HT** HTM-based devices with a Li salt and TBP resulted in nearly 60-fold improvement in device efficiency [25]. Before being spin-coated onto **D102**-sensitized $TiO_2$ electrodes, the HTM solutions were filtered on 0.2 μm Millipore.

In view of analysing the load of the **D102** dye adsorbed on the $TiO_2$ electrodes and the effect of the HTM on the absorption profile, UV–visible absorption spectra were recorded (Fig. 1). The **D102**/**P3HT** system displays a different absorption profile

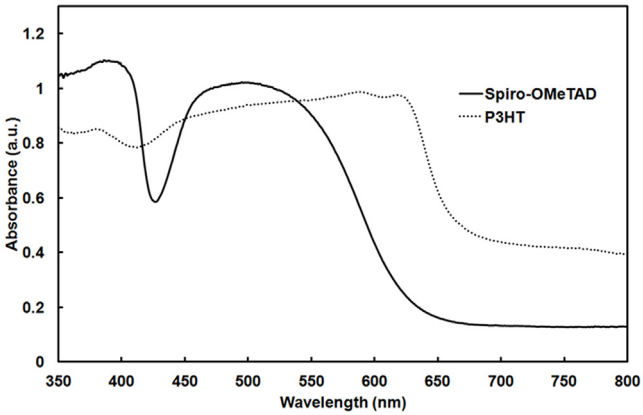


**Fig. 1.** UV–vis absorption spectra of **D102**/**spiro-OMeTAD** (solid line) and **D102**/**P3HT** (dotted line) based ss-DSSCs.

compared to **D102**/**spiro-OMeTAD**, as observed with the naked eye (Fig. S3, ESI). Generally, when **P3HT** is applied as HTM in ss-DSSCs, only a small increase in absorbance is generally observed indicating its weak infiltration into the $TiO_2$ layer [29,44]. This poor pore filling ability of the **P3HT** HTM material commonly implies lower performances than **spiro-OMeTAD** [43]. In our case, the absorbance values are almost the same as with **spiro-OMeTAD** but the profile is significantly broadened between 550 and 650 nm. This extended absorption with the emergence of a vibronic structure between 550 nm and 650 nm suggests that P3HT self-assembled into a lamellar-like structure built from interchain π–π interactions between the planarized aromatic backbones of the polymer chains [45]. This observation is quite important since the formation of ordered nanostructures is crucial for efficient hole transport [46].

The photocurrent density voltage curves (J-V) of the devices employing **D102** as dye and **spiro-OMeTAD** or **P3HT** as HTM are presented in Figs. 2 and S4-5 in the Supporting Information. The photovoltaic parameters are collected in Table 1 before and after applying a post-infiltration annealing treatment to the HTM-infiltrated devices, prior to electrode deposition. The performances obtained for the reference cells based on **D102** and **spiro-OMeTAD**, before and after annealing, are consistent with those previously reported in the literature [33,34]. Interestingly, we observed that **P3HT** gives a similar efficiency than **spiro-OMeTAD** when used with **D102** (PCE = 3.90% *vs.* PCE = 3.93%),

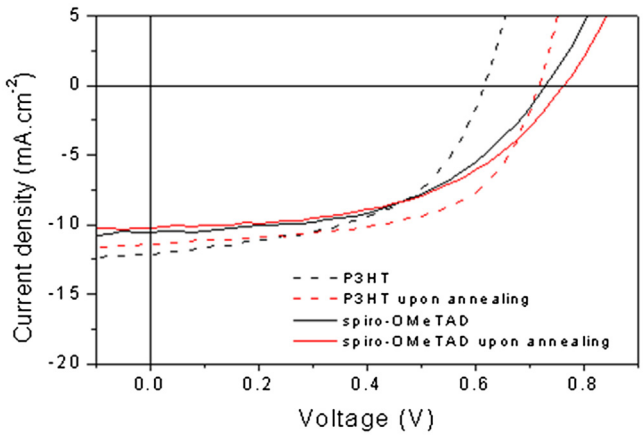


**Fig. 2.** Current-voltage characteristics of ss-DSSCs sensitized with **D102** depending on the HTM: **spiro-OMeTAD** (solid black line), **P3HT** (dash black line) and upon annealing (both respective red lines). (For interpretation of the references to colour in this figure legend, the reader is referred to the web version of this article.)

**Table 1**
Photovoltaic parameters of ss-DSSCs sensitized with **D102** under simulated solar emission as a function of the HTM: short-circuit current density ($J_{SC}$), open-circuit voltage ($V_{OC}$); fill factor (FF) and power conversion efficiency ($\eta$). [a]Annealing procedure: 150 °C/5 min.

| HTM | $V_{OC}$ (V) | $J_{SC}$ (mA cm$^{-2}$) | FF | Average $\eta$ (%) |
|---|---|---|---|---|
| spiro-OMeTAD | 0.73 | 10.52 | 0.51 | 3.90 |
| Annealed spiro-OMeTAD[a] | 0.76 | 10.21 | 0.51 | 3.99 |
| P3HT | 0.62 | 12.14 | 0.52 | 3.93 |
| Annealed P3HT[a] | 0.72 | 11.37 | 0.58 | 4.78 |

before the annealing treatment. Regarding the other photovoltaic parameters, both types of devices show similar FF (52% for **P3HT** *vs.* 51% for **spiro-OMeTAD**), but different $J_{SC}$ and $V_{OC}$ values. **P3HT** provides a better photocurrent (about 15% higher), which suggests better charge transport properties [29].

To our knowledge, this is the first example where **P3HT** shows such remarkable results when associated with relatively thick $TiO_2$ electrodes (around 2 μm). Indeed, ss-DSSCs with **P3HT** as HTM usually exhibit modest performances due to the poor pore-filling of **P3HT** into mesoporous $TiO_2$ film [47]. Taking into account this incomplete pore-filling, several research groups showed that the enhancement of device performances could be achieved by decreasing the $TiO_2$ layer thickness [48,49].

However, it is worth noting that in most cases, the **P3HTs** used in those reports are commercial polymers, with higher molecular weights (up to 50 kDa) and dispersities (>1.5) [48,50]. Recently, Wang et al. have shown that **P3HT** with high molecular weight (≈60 kDa) results in non-uniform infiltration into the $TiO_2$ mesoporous layer and thus, decreased device performances [42].

The optoelectronic properties of **P3HT** are known to be strongly related to the polymer regioregularity, the molecular weight and the dispersity [51,52]. Snaith et al. illustrated this effect by studying regiorandom and regioregular **P3HT** as HTM in ss-DSSCs [53]. As expected, due to its higher crystalline character, more suitable to charge transport, regioregular **P3HT** yielded a better efficiency compared to regiorandom P3HT (1.7% *vs.* 0.54%, respectively). Recently, Salleo et al. reported that a large polymer dispersity is detrimental to the charge transport properties, due to molecular mixing of high and low molecular weight chains, which reduces the density of aggregate-connecting molecules [54]. Since the KCTP method enables to obtain **P3HT** with a controlled molecular weight, narrow dispersity and high regioregularity, better pore-filling, organization and hole mobility may be expected from our **P3HT** ($M_n$ = 23 000 g mol$^{-1}$, Đ = 1.24, RR > 97%) compared to commercial polymers, which would provide better performances in ss-DSSCs.

The incident photon to electron conversion efficiency (IPCE) recorded for the ss-DSSCs described above shows that the photocurrent response of the **P3HT** devices is higher than that of **spiro-OMeTAD** devices, with maximum peak values of 72 and 68% at 480 and 475 nm, respectively (Fig. 3). These maxima are coherent with the values of the short-circuit current observed in both **spiro-OMeTAD** and **P3HT** based ss-DSSCs (10.52 *vs.* 12.14 mA/cm$^2$). This indicates that the charge generation process is extremely efficient in ss-DSSC with **P3HT** as HTM. To further investigate the infiltration of **P3HT** and **spiro-OMeTAD** into the dye-sensitized $TiO_2$ electrodes, SEM analyses were performed on cross-sections of the samples (Fig. 4). Over the glass substrate (bottom), the layers that compose the cell, *i.e.* the conducting FTO, the dense spray-pyrolyzed $TiO_2$ layer, the mesoporous $TiO_2$ layer and the electrode, can be distinguished. The HTM materials are homogenously distributed for both **P3HT** and **spiro-OMeTAD**-based solar cells. Interestingly, the cell filled with **P3HT** seems to present a good infiltration into the mesoporous $TiO_2$ layer down to the bottom of the electrode. The molecular characteristics of the

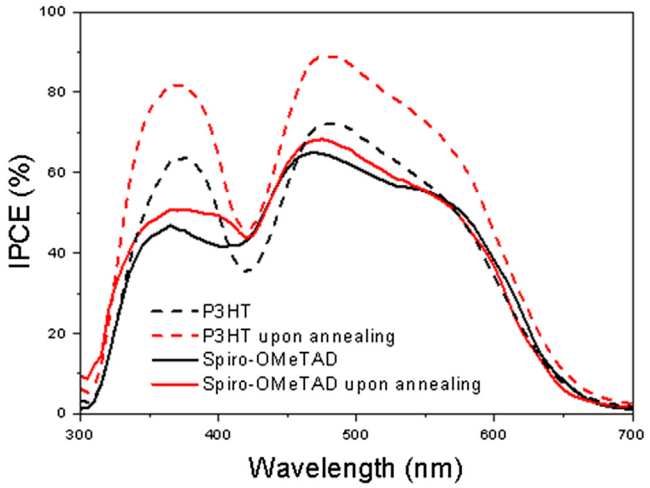


**Fig. 3.** IPCE spectra of ss-DSSCs based on dye D102 depending on the HTM layer.

**P3HT** (*i.e.*, medium-range molecular weight of 23 000 g mol$^{-1}$ and narrow dispersity of 1.24) seem to be really adequate to its infiltration into the $TiO_2$ mesopores, thus leading to excellent performances when used as HTM in **D102**-based ss-DSSCs.

Regioregular **P3HT** is known to form fibrillar (nanowire-like) crystallites that arrange in lamellae in thin films. The hole mobility in **P3HT** is also known to substantially increase upon annealing [55–57]. Thus, thermal annealing at 150 °C for 5 min was carried out before the evaporation of Au electrodes in order to improve the device performances. As shown in Fig. 2 and Table 1, PCE was improved up to an absolute value of 4.8%, corresponding to a relative increase of about 20% compared to the non-annealed devices. In the same conditions, the performances of solar cells based on **spiro-OMeTAD** only increased by a relative factor of 2%. It was already shown that the LiTFSI additive can induce **spiro-OMeTAD** oxidation upon high thermal annealing temperatures, which becomes detrimental for device operation [58]. For solar cells based on **P3HT**, $V_{OC}$ and FF increased significantly from 0.62 to 0.72 V and 52 to 58% on average, respectively. Therefore, we assume that the enhancement in device performances is related to the strong influence of annealing on the **P3HT** charge transport properties, through the morphology of the HTM.

To verify this assumption, AFM images were recorded on non-annealed and annealed **P3HT**-based device and compared to the **spiro-OMeTAD**-based devices (Fig. 5). The devices filled with **spiro-OMeTAD** exhibit a granular morphology characteristic of the $TiO_2$ mesoporous structure and an average roughness of 7.2 nm, suggesting a quite flat and compact HTM overlayer (Fig. 5a). It is important to note that no significant change is observed regarding the morphology in spiro-OMeTAD device whatever the treatment. In contrast, the formation of larger grains is observed for the devices infiltrated with **P3HT**, which is accompanied by an increase in film thickness and surface roughness (∼19.5 nm) (Fig. 5b). Upon annealing at 150 °C, the morphology of the **P3HT** film shows a higher content of fibrillar structures (*i.e.*, it becomes more crystalline), which is expected to improve the local charge carrier mobility (Fig. 5c and d) [39,40].

To further understand the annealing-induced enhancement in PCE, hole mobility measurements were performed on neat **P3HT** and **spiro-OMeTAD** layers using simple bottom gate/bottom contact field-effect transistors in ambient conditions (see experimental details and Fig. S6-7, ESI). As expected, the hole mobility of **P3HT** was found to be much higher than that of **spiro-OMeTAD**, *i.e.*, $10^{-3}$ *vs.* $10^{-5}$ cm$^2$ s$^{-1}$ V$^{-1}$, whatever the treatment used (Table S2, ESI). Upon thermal annealing at 80 °C, the hole mobility of **P3HT**

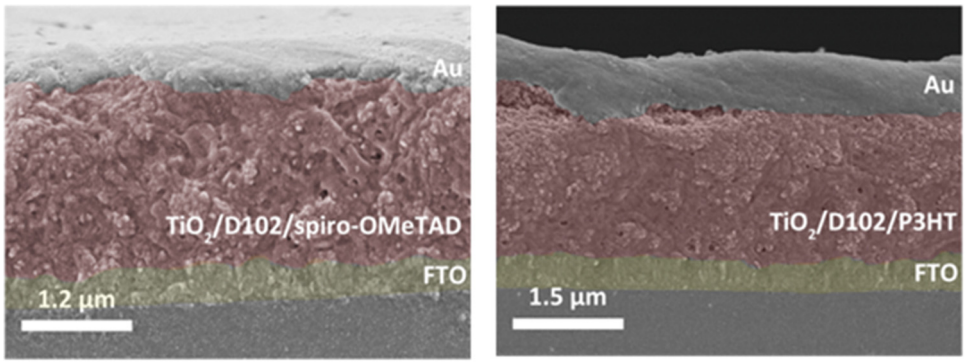


**Fig. 4.** Cross-sectional SEM images of ss-DSSCs sensitized with **D102** depending on the HTM: **spiro-OMeTAD** (left) and **P3HT** (right).

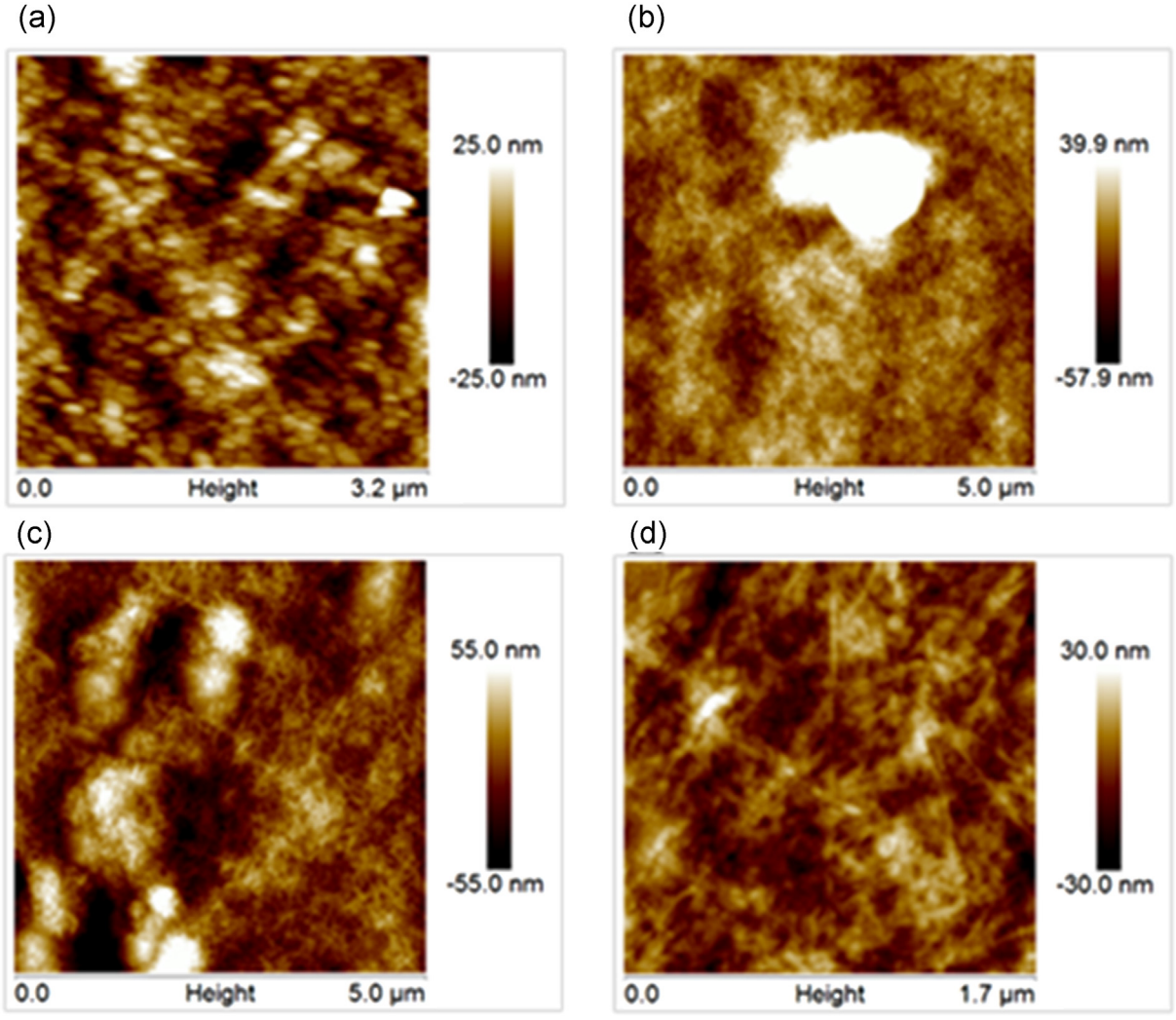


**Fig. 5.** Tapping-Mode AFM height images of (a) annealed **spiro-OMeTAD** device, (b) a **P3HT** device without annealing, (c, d) a **P3HT** device after thermal annealing; (d) is a zoom of (c).

increased by about 40%. Thus, the **P3HT** annealed up to 150 °C may exhibit an increased field effect mobility compared with as-prepared devices, as already reported [55,56]. The values of the series resistances of the devices also show a decrease by about 10% after thermal treatment (Table S1, ESI). These better charge transport properties are also expected to reduce the interfacial charge recombination mechanisms. Consistently, better open-circuit voltage and fill factor values are indeed observed for the annealed **P3HT** ss-DSSC devices.

The positive influence of **P3HT** annealing on hole transport and device performance being rationalized, the apparent discrepancy between the IPCE spectra and the photovoltaic measurements was examined. Indeed, a significant increase of photocurrent generation is noticed after annealing for **P3HT** devices (Fig. 3) whereas

the experimental Jsc values measured under simulated solar emission (Table 1) show a small decrease after annealing (~5%). This behavior is quite different from that of the **spiro-OMeTAD** devices, which show similar values of IPCE and experimental short-circuit current densities before or after annealing. As the IPCE was recorded without any background continuous white bias illumination, the data indicate that a light-dependent mechanism is occurring for **P3HT**-based devices. Fig. 6 presents the photocurrent density $J_{ph}$ defined as the difference between the current densities obtained under standard illumination at 100 mW cm$^{-2}$ ($J_{sun}$) and in the dark ($J_{dark}$), as a function of the effective applied voltage ($V_{eff} = V_{bi} - V$), where $V_{bi}$ is the built-in potential defined by $J_{dark}(V_{bi}) = J_{sun}(V_{bi})$ [56].

This double logarithmic plot emphasizes the limitations to charge collection in the device as a function of the effective applied voltage, under simulated sunlight. This approach was indeed useful to explore the main physical processes governing polymer: fullerene bulk heterojunctions, including drift and diffusion of charge carriers, charge carrier generation, and recombination [59]. Basically, the plot shows two transport regimes for photogenerated carriers: the first one at low effective bias voltage is governed by generation-recombination mechanisms in the bulk, while the second regime at high effective bias voltage, where recombination is not efficient, is governed only by drift diffusion through the bulk. Thus, at the voltage threshold between these two regimes, all the available photogenerated charges carriers are extracted from the device so that the photocurrent density is directly linked to the photogenerated charge carrier density in the bulk. Here, it is clearly seen that this carrier density is almost the same for all devices so that differences between these devices must be attributed to mobility limitation by traps. Despite quite similar short-circuit current densities for all devices (corresponding to effective voltage of around 0.8 V), the pseudo saturation regime for $J_{ph}$ is reached at lower effective voltage for the annealed **P3HT** devices (~0.23 V), compared to untreated or annealed **spiro-OMeTAD** (around 0.29 V in both cases) and untreated **P3HT** (~0.44 V). This behavior is consistent with the trend in device performance and illustrates the intrinsic trap-limited transport occurring in **P3HT**. This observation is also coherent with the evolution of $J_{ph}$ in the linear regime ($V_{eff} < 0.1\ V$), which evidences specific limitations for **P3HT** before annealing compared to **spiro-OMeTAD** and annealed **P3HT**. Such findings are fully consistent with the positive influence of annealing on the morphology and charge transport properties of **P3HT**. Charge transport and recombination are directly related to the fill factor [60]. Thus, by improving charge transport and reducing trap-assisted recombination after annealing, the fill factor strongly increases, as observed for annealed **P3HT** (Table 1).

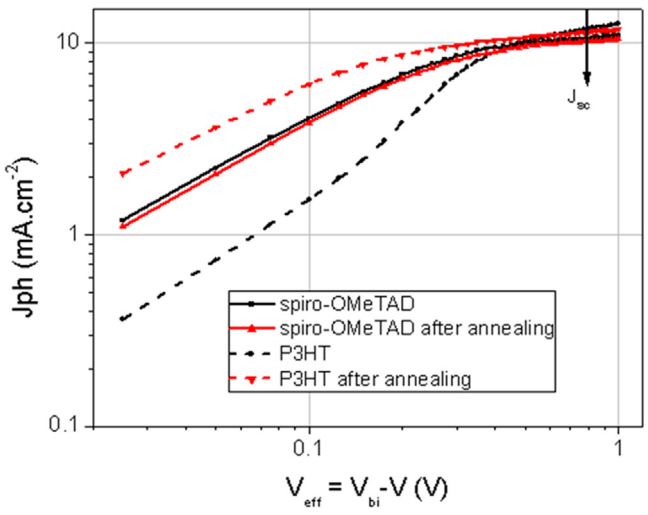


**Fig. 6.** Photocurrent as a function of the effective applied voltage for cells based on **spiro-OMeTAD** (solid lines) and **P3HT** (dashed lines), before (black) and after (grey) annealing.

Nevertheless, no square-root dependence of $J_{ph}$ versus the effective voltage is evidenced, which indicates that the photocurrent is not limited by a space-charge build-up [57,61]. Therefore, our analysis suggests that the diffusion (low $V_{eff}$ values) and drift (for large $V_{eff}$) of photo-generated charge carriers are trap-limited in pristine **P3HT**, due to its poor structuration. These traps, which are largely cured through thermal annealing, are also highly dependent on the illumination conditions. Under low light intensities, such as those encountered during IPCE measurements (around 5 mW cm$^{-2}$), the extracted photocurrent is strongly limited by the trap distribution associated with pristine **P3HT**, through an effective trap-limited hole mobility. The full extraction of charge carriers would therefore require a larger effective applied potential, or the application of a high intensity bias illumination. At the opposite, the annealed **P3HT**, which does not exhibit the same trap-limitation due to its thermal structuration, delivers its maximal photocurrent, both under low and high light conditions. A significant increase of IPCE is therefore observed in this case after annealing. In contrast, the charge transport properties of **spiro-OMeTAD**, which is a molecular glass material, are not sensitive to annealing in the range of temperatures used in this work. Annealing only slightly affects its configuration in the pores of the electrode.

## 4. Conclusions

All solid-state dye-sensitized solar cells based on poly(3-hexylthiophene) (**P3HT**) as hole transporting material (HTM) were prepared and their performances were compared to **spiro-OMeTAD**. Highly regioregular **P3HT** with narrow dispersity, synthesized using the KCTP method, enables to reach high PCEs up to 4.78% (*vs.* 3.99% for **spiro-OMeTAD**), after an additional annealing step. This is, to the best of our knowledge, the first report where **P3HT** shows better performances than **spiro-OMeTAD** as HTM in ss-DSSCs. A careful choice of the polymer molecular characteristics (high regioregularity, medium-range molecular weight and narrow dispersity) combined with appropriate thermal annealing are required to achieve high hole mobility and thus, improved charge extraction efficiency. Probably, the well-defined, medium-range **P3HT** used in this work represents a good compromise between crystallinity, charge transport and infiltration. This finding deserves further studies to gain deeper insight into the effects of the molecular weight of the polymer, the use of additives or the nature of the dyes, which will provide new insights in the use of **P3HT** as HTM in ss-DSSCs.

## Acknowledgements

The authors thank the CNRS and the Université de Montpellier for financial support. Research in Mons is supported by the Science Policy Office of the Belgian Federal Government (BELSPO; PAI 7/05), FNRS-FRFC and the 'Actions de Recherche Concertée' programme (MADSSCELLS project). M.S. is research associate of the FNRS. The authors are also grateful to the "SATT Grand Centre" for financial support. The authors thank also Didier Cot (Université de Montpellier) for his help in SEM measurements. FNRS is also acknowledged for a visiting professor grant for S.C.

## Appendix A. Supplementary data

$^{1}$H NMR spectrum and SEC profile of **P3HT, IPCE** spectra and current density-voltage of **D102**-based ss-DSSCs in the dark, series

resistance calculated for **P3HT** and **spiro-OMeTAD**-based ss-DSSCs, mobility values for **P3HT** and **spiro-OMeTAD**-based OFETs, output and transfer characteristics of **P3HT**-based OFETs upon thermal annealing.

Supplementary data associated with this article can be found, in the online version, at http://dx.doi.org/10.1016/j.synthmet.2017.02.015.

## References


[1] J. Zhao, A. Wang, M.A. Green, Sol. Energy Mater. Sol. Cells 66 (2001) 27–36.
[2] T. Saga, NPG Asia Mater. 2 (2010) 96–102.
[3] B.C. O'Regan, M. Grätzel, Nature 353 (1991) 737–740.
[4] H.S. Jung, J.-K. Lee, J. Phys. Chem. Lett. 4 (2013) 1682–1693.
[5] S. Mathew, A. Yella, P. Gao, R. Humphry-Baker, B.F. Curchod, N. Ashari-Astani, I. Tavernelli, U. Rothlisberger, M.K. Nazeeruddin, M. Grätzel, Nat. Chem. 6 (2014) 242–247.
[6] S.M. Feldt, E.A. Gibson, E. Gabrielsson, L. Sun, G. Boschloo, A. Hagfeldt, J. Am. Chem. Soc. 132 (2010) 16714–16724.
[7] S.A. Sapp, C.M. Elliott, C. Contado, S. Caramori, C.A. Bignozzi, J. Am. Chem. Soc. 124 (2002) 11215–11222.
[8] Y. Bai, Q. Yu, N. Cai, Y. Wang, M. Zhanga, P. Wang, Chem. Commun. 47 (2011) 4376–4378.
[9] B.E. Hardin, H.J. Snaith, M.D. McGehee, Nat. Photon. 6 (2012) 162–169.
[10] P. Wang, S.M. Zakeeruddin, J.E. Moser, M.K. Nazeeruddin, T. Sekiguchi, M. Grätzel, Nat. Mater. 2 (2003) 402–407.
[11] B. Li, L. Wang, B. Kang, P. Wang, Y. Qiu, Sol. Energy Mater. Sol. Cells 90 (2006) 549–562.
[12] M. Zakeeruddin, M. Grätzel, Adv. Funct. Mater. 19 (2009) 2187–2202.
[13] J. Wu, Z. Lan, J. Lin, M. Huang, Y. Huang, L. Fan, G. Luo, Chem. Rev. 115 (2015) 2136–2173.
[14] U. Bach, K.D. Cloedt, H. Spreitizer, M. Grätzel, Adv. Mater. 12 (2000) 1060–1063.
[15] J. Burschka, A. Dualeh, F. Kessler, E. Baranoff, N.-L. Cevey-Ha, C. Yi, M.K. Nazeeruddin, M. Grätzel, J. Am. Chem. Soc. 133 (2011) 18042–18045.
[16] D. Poplavskyy, J. Nelson, J. Appl. Phys. 93 (2003) 341–346.
[17] I.-K. Ding, J. Melas-Kyriazi, N.-L. Cevey-Ha, K.G. Chittibabu, S.M. Zakeeruddin, M. Grätzel, M.D. McGehee, Org. Electron. 11 (2010) 1217–1222.
[18] S.X. Tan, J. Zhai, M.X. Wan, L. Jiang, B.D. Zhu, Synth. Met. 137 (2003) 1511–1512.
[19] Y. Duan, Q. Tang, Y. Chen, Z. Zhao, Y. Lv, M. Hou, P. Yang, B. He, L. Yu, J. Mater. Chem. A 3 (2015) 5368–5374.
[20] R. Cervini, Y. Cheng, G. Simon, J. Phys. D: Appl. Phys. 37 (2004) 13–20.
[21] T. Kitamura, M. Maitani, M. Matsuda, Y. Wada, S. Yanagida, Chem. Lett. 30 (2001) 1054–1055.
[22] J. Kim, J. Koh, B. Kim, E. Kim, Angew. Chem. Int. Ed. 51 (2012) 6864–6869.
[23] J. Xia, N. Masaki, M. Lira-Cantu, Y. Kim, K. Jiang, S. Yanagida, J. Am. Chem. Soc. 130 (2008) 1258–1263.
[24] J. Zhang, L. Yang, Y. Shen, B.-W. Park, Y. Hao, E.M. Johansson, G. Boschloo, L. Kloo, E. Gabrielsson, L. Sun, J. Phys. Chem. C 118 (2014) 16591–16601.
[25] R. Zhu, C. Jiang, B. Liu, S. Ramakrishna, Adv. Mater. 21 (2009) 994–1000.
[26] W. Zhang, R. Zhu, F. Li, Q. Wang, B. Liu, J. Phys. Chem. C 115 (2011) 7038–7043.
[27] H. Sirringhaus, P.J. Brown, R.H. Friend, M.M. Nielsen, K. Bechgaard, B.M.W. Langeveld-Voss, A.J.H. Spiering, R.A.J. Janssen, E.W. Meijer, P. Herwig, D.M. de Leeuw, Nature 401 (1999) 685–688.
[28] R.J. Kline, M.D. McGehee, E.N. Kadnikova, J.S. Liu, J.M.J. Frechet, Adv. Mater. 15 (2003) 1519–1522.
[29] S.-J. Moon, E. Baranogg, S.M. Zakeeruddin, C.-Y. Yeh, E.W.-G. Diau, M. Grätzel, K. Sivula, Chem. Commun. 47 (2011) 8244–8246.
[30] L. Yang, U.B. Cappel, E.L. Unger, M. Karlsson, K.M. Karlsson, E. Gabrielsson, L. Sun, G. Boschloo, A. Hagfeldt, E.M.J. Johansson, Phys. Chem. Chem. Phys. 14 (2012) 779–789.
[31] J. Melas-Kyriazi, I.K. Ding, A. Marchioro, A. Punzi, B.E. Hardin, G.F. Burkhard, N. Tétreault, M. Grätzel, J.-E. Moser, M.D. McGehee, Adv. Energy Mater. 1 (2011) 407–414.
[32] T. Horiuchi, H. Miura, K. Sumioka, S. Uchida, J. Am. Chem. Soc. 126 (2004) 12218–12219.
[33] L. Schmidt-Mende, U. Bach, R. Humphry-Baker, T. Horiuchi, M. Miura, S. Ito, S. Uchida, M. Grätzel, Adv. Mater. 17 (2005) 813–815.
[34] H. Melhem, P. Simon, L. Beouch, F. Goubard, M. Boucharef, C. Di Bin, Y. Leconte, B. Ratier, N. Herlin-Boime, J. Bouclé, Adv. Energy Mater. 1 (2011) 908–916.
[35] F. Boon, S. Desbief, L. Cutaia, O. Douhéret, A. Minoia, B. Ruelle, S. Clément, O. Coulembier, J. Cornil, P. Dubois, R. Lazzaroni, Macromol. Rapid Commun. 31 (2010) 1427–1434.
[36] M. Chevrier, S. Richeter, O. Coulembier, M. Surin, A. Mehdi, R. Lazzaroni, R.C. Evans, P. Dubois, S. Clément, Chem. Commun. 52 (2016) 171–174.
[37] M. Trznadel, A. Pron, M. Zagorska, R. Chrzaszcz, J. Pielichowski, Macromolecules 31 (1998) 5051–5058.
[38] R.J. Kline, M.D. McGehee, E.N. Kadnikova, J. Liu, J.M. Frechet, M.F. Toney, Macromolecules 38 (2005) 3312–3319.
[39] A. Zen, M. Saphiannikova, D. Neher, G. Wegner, Macromolecules 39 (2006) 2162–2171.
[40] F. Panzer, H. Bassler, R. Lohwasser, M. Thelakkat, A. Kohler, J. Phys. Chem. Lett. 5 (2014) 2742–2747.
[41] I. Osaka, R.D. McCullough, Acc. Chem. Res. 41 (2008) 1202–1214.
[42] Y. Zhang, K. Cao, X. Zhu, X. Li, X. Qiao, G. Tu, B. Zhang, D. Huang, Y. Shen, M. Wang, RSC Adv. 3 (2013) 14037–14043.
[43] A. Abrusci, S. Kumar, R. Sai, M. Al-Hashimi, M. Heeney, A. Petrozza, H.J. Snaith, Adv. Funct. Mater. 21 (2011) 2571–2579.
[44] K.M. Coakley, M.D. McGehee, Chem. Mater. 16 (2004) 4533–4542.
[45] W.D. Oosterbaan, V. Vrindts, S. Berson, S. Guillerez, O. Douhéret, B. Ruttens, J. D'Haen, P. Adriaensens, J. Manca, L. Lutsen, D. Vanderzande, J. Mater. Chem. 19 (2009) 5424–5435.
[46] M.-C. Chen, W.-C. Hung, A.-C. Su, S.-H. Chen, S.-A. Chen, J. Phys. Chem. B 113 (2009) 11124–11133.
[47] J. Bouclé, J. Ackermann, Polym. Int. 61 (2012) 355–373.
[48] H.J. Snaith, A.J. Moule, C. Klein, K. Meerholz, R.H. Friend, M. Grätzel, Nano Lett. 7 (2007) 3372–3376.
[49] M. Wang, M. Xu, D. Shi, R. Li, F. Cao, G. Zhang, Z. Yi, R. Humphry-Baker, P. Wang, S.M. Zakeeruddin, M. Grätzel, Adv. Mater. 20 (2008) 4460–4463.
[50] A. Dupuis, P. Wong-Wah-Chung, A. Rivaton, J.-L. Gardette, Polym. Degrad. Stab. 97 (2012) 366–374.
[51] R.C. Hiorns, R. de Bettignies, J. Leroy, S. Bailly, M. Firon, C. Sentein, A. Khoukh, H. Preud'homme, C. Dagron-Lartigau, Adv. Funct. Mater. 16 (2006) 2263–2273.
[52] A.M. Ballantyne, L. Chen, J. Dane, T. Hammant, F.M. Braun, M. Heeney, W. Duffy, I. McCulloch, D.D.C. Bradley, J. Nelson, Adv. Funct. Mater. 18 (2008) 2373–2380.
[53] R. Sai Santosh Kumar, G. Grancini, A. Petrozza, A. Abrusci, H.J. Snaith, G. Lanzani, Opt. Express 21 (2013) A469–A474.
[54] S. Himmelberger, K. Vandewal, Z. Fei, M. Heeney, A. Salleo, Macromolecules 47 (2014) 7151–7157.
[55] A. Zen, J. Pflaum, S. Hirschmann, W. Zhuang, F. Jaiser, U. Asawapirom, J.P. Rabe, U. Scherf, D. Neher, Adv. Funct. Mater. 14 (2004) 757–764.
[56] S. Cho, K. Lee, J. Yuen, G. Wang, D. Moses, A.J. Heeger, M. Surin, R. Lazzaroni, J. Appl. Phys. 100 (2006) 114503/1-114503/6.
[57] V.D. Mihailetchi, H. Xie, B. de Boer, L.J.A. Koster, P.W.M. Blom, Adv. Funct. Mater. 16 (2006) 699–708.
[58] Y. Fang, Xi. Wang, Q. Wang, J. Huang, T. Wu, Phys. Status Solidi A 211 (2014) 2809–2816.
[59] L.J.A. Koster, E.C.P. Smits, V.D. Mihailetchi, P.W.M. Blom, Phys. Rev. B 72 (2005) 085205.
[60] D. Bartesaghi, I. del Carmen Pérez, J. Kniepert, S. Roland, M. Turbiez, D. Neher, L. Jan Anton Koster, Nat. Commun. 6 (2015) 7083.
[61] V.D. Mihailetchi, J. Wildeman, P.W.M. Blom, Phys. Rev. Lett. 94 (2005) 126602.